Mineralogical Magazine (2021), **85**, 862–867
doi:10.1180/mgm.2021.75

CAMBRIDGE UNIVERSITY PRESS

Article

Whiteite-(MnMnMn), a new jahnsite-group mineral species from the Foote mine, North Carolina, USA, and chemical pressure effects in jahnsite-group minerals.

Ian E. Grey[1]*, Jason B. Smith[2], Anthony R. Kampf[3], W. Gus Mumme[1], Colin M. MacRae[1], Alan Riboldi-Tunnicliffe[4], Stephanie Boer[4], Alexander M. Glenn[1] and Robert W. Gable[5]

[1]CSIRO Mineral Resources, Private Bag 10, Clayton South, Victoria 3169, Australia; [2]2148 McClintock Road, Charlotte, NC 28205, USA; [3]Mineral Sciences Department, Natural History Museum of Los Angeles County, 900 Exposition Boulevard, Los Angeles, CA 90007, USA; [4]Australian Synchrotron, 800 Blackburn Road, Clayton, Victoria 3168, Australia; and [5]School of Chemistry, University of Melbourne, Parkville, Victoria 3010, Australia.

Abstract

Whiteite-(MnMnMn), $Mn^{2+}Mn^{2+}Mn^{2+}_2Al_2(PO_4)_4(OH)_2{\cdot}8H_2O$, is a new whiteite-subgroup member of the jahnsite group from the Foote Lithium Company mine, Kings Mountain district, Cleveland County, North Carolina, USA. It was found in small vugs of partially oxidised pegmatite minerals on the East dump of the mine, in association with eosphorite, hureaulite, fairfieldite, mangangordonite, whiteite-(CaMnMn) and jasonsmithite. It occurs as sugary aggregates of blade-like crystals up to 0.1 mm long and as epitaxial overgrowths on whiteite-(CaMnMn). The crystals are colourless to very pale brown, with a vitreous lustre and a white streak. The blades are flattened on {001} and elongated along [010], with poor cleavage on {001}. The calculated density is 2.82 g·cm^{-3}. Optically it is biaxial (–) with $\alpha = 1.599(2)$, $\beta = 1.605(2)$, $\gamma = 1.609(2)$ (white light); 2V (calc.) = 78.2°, having no observable dispersion or pleochroism, and with orientation $X = \mathbf{b}$. Electron microprobe analyses and structure refinement gave the empirical formula $(Mn^{2+}_{0.59}Ca_{0.38}Na_{0.03})_{\Sigma 1.00}Mn_{1.00}(Mn^{2+}_{1.04}Fe^{3+}_{0.58}Fe^{2+}_{0.23}Zn_{0.16}Mg_{0.08})_{\Sigma 2.09}Al_{2.04}(PO_4)_{3.89}(OH)_{3.18}(H_2O)_{7.26}$. Whiteite-(MnMnMn) is monoclinic, P2/*a*, $a = 15.024(3)$ Å, $b = 6.9470(14)$ Å, $c = 9.999(2)$ Å, $\beta = 110.71(3)°$, $V = 976.2(4)$ Å^3 and $Z = 2$. The crystal structure was refined using synchrotron single-crystal data to $wR_{obs} = 0.057$ for 2014 reflections with $I > 3\sigma(I)$. Site occupancy refinements confirm the ordering of dominant Mn in the *X*, *M*1 and *M*2 sites of the general jahnsite-group formula $XM1(M2)_2(M3)_2(H_2O)_8(OH)_2(PO_4)_4$. A review of published crystallochemical data for jahnsite-group minerals shows a consistent chemical pressure effect in these minerals, manifested as a contraction of the unit-cell parameter, *a*, as the mean size of the *X* and *M*1 site cations increases. This is analogous to negative thermal expansion, but with increasing cation size, rather than heating, inducing octahedral rotations that result in an anisotropic contraction of the unit cell.

Keywords: whiteite-(MnMnMn), new jahnsite-group mineral, crystal structure, chemical pressure

(Received 12 August 2021; accepted 30 September 2021; Accepted Manuscript published online: 18 October 2021; Associate Editor: Oleg I Siidra)

Introduction

Recently, Kampf *et al.* (2019) obtained formal approval by the International Mineralogical Association (IMA) Commission on New Minerals, Nomenclature and Classification (CNMNC) for a nomenclature system for jahnsite-group minerals, originally proposed by Moore and Ito (1978). The general formula for these minerals is $XM1(M2)_2(M3)_2(H_2O)_8(OH)_2(PO_4)_4$, where minerals with $M3 = Fe^{3+}$ form the jahnsite subgroup and those with $M3 = Al^{3+}$ form the whiteite subgroup. Within the two subgroups, different species are distinguished by the dominant cations in the *X*, *M*1 and *M*2 sites, represented by a suffix -(*XM*1*M*2) in the mineral name. It has been generally observed that the mean sizes of these cations are in the order $X > M1 > M2$, (Moore and Ito, 1978; Kampf *et al.*, 2019) and this observation has been used to define and name new species where site assignments cannot be made unambiguously from crystal structure refinements (Grey *et al.*, 2020). To date, 12 jahnsite-subgroup members have been officially approved by the IMA but only seven whiteite-subgroup members have been approved. We report here the characterisation of an eighth member of the whiteite subgroup, whiteite-(MnMnMn), from the Foote Lithium Company mine, North Carolina, USA. The mineral and name were approved by the IMA-CNMNC (IMA2021-049, Grey *et al.*, 2021). Four co-type specimens from the Foote mine are housed in the mineralogical collections of the Natural History Museum of Los Angeles County, catalogue numbers 74374, 76149, 76150 and 76151. The specimen number 74374 is also the holotype for jasonsmithite (Kampf *et al.*, 2021).

*Author for correspondence: Ian E. Grey, Email: ian.grey@csiro.au
Cite this article: Grey I.E., Smith J.B., Kampf A.R., Mumme W.G., MacRae C.M., Riboldi-Tunnicliffe A., Boer S., Glenn A.M. and Gable R.W. (2021) Whiteite-(MnMnMn), a new jahnsite-group mineral species from the Foote mine, North Carolina, USA, and chemical pressure effects in jahnsite-group minerals.. *Mineralogical Magazine* **85**, 862–867. https://doi.org/10.1180/mgm.2021.75

Fig. 1. Whiteite-(MnMnMn) from the Foote mine. Field of view is 1.3 mm. JBS personal collection specimen 7246F.

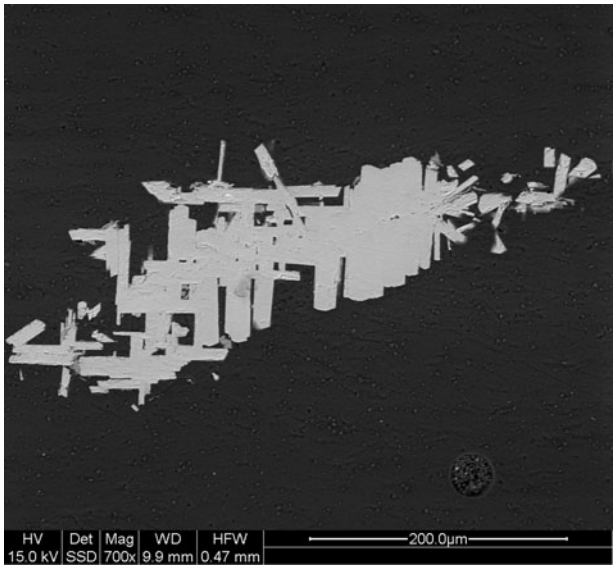

Fig. 2. Back-scattered electron image of whiteite-(MnMnMn) crystals showing orthogonal orientation. Natural History Museum of Los Angeles County specimen 76151.

Occurrence and paragenesis

Whiteite-(MnMnMn) was found by one of the authors (JBS) in small vugs of a float boulder on the East dump of the Foote Lithium Company mine, Kings Mountain district, Cleveland County, North Carolina, USA (35°12'40"N, 81°21'20"W). The boulder had been excavated from an upper, partially oxidised and altered part of the pegmatite, where ground water had penetrated the pegmatite along natural fractures and leached primary and secondary minerals such as fluorapatite and fairfieldite. The diverse suite of tertiary phosphate mineralisation formed in cavities left behind by the leached primary fluorapatite, and along the aforementioned natural fractures. The pegmatite matrix comprises albite, columbite-(Fe), ferrisicklerite, fluorapatite, muscovite, quartz, sphalerite and spodumene. The associated minerals, in order of formation, are eosphorite, hureaulite, fairfieldite, jasonsmithite, mangangordonite and whiteite-(CaMnMn), with whiteite-(MnMnMn) being the last to form. Its common presence as orthogonally oriented laths on whiteite-(CaMnMn), suggests a dissolution/epitaxial recrystallisation paragenesis. The Foote Lithium Company mine is the type locality for 15 other minerals, including jasonsmithite, which was found in the same boulder as whiteite-(MnMnMn) (Kampf *et al.*, 2021).

Table 1. Analytical data (wt.%) for whiteite-(MnMnMn).

Constituent	Mean	Range	S.D.	Standard
CaO	2.58	1.81–3.87	0.51	Apatite
Na_2O	0.11	0.00–0.35	0.18	albite
MnO	22.8	21.7–23.6	0.63	wollastonite
ZnO	1.62	1.08–2.43	0.44	phosphophyllite
MgO	0.40	0.18–0.62	0.13	spinel
Al_2O_3	12.7	11.9–13.4	0.46	berlinite
Fe_2O_3 (total)	(7.98)	6.86–9.07	0.67	hematite
FeO	2.05			
Fe_2O_3	5.70			
P_2O_5	33.7	32.4–35.0	0.82	berlinite
H_2O*	19.5			
Total	101.16			

*Based on the crystal structure (O = 26)
S.D. – standard deviation

Physical and optical properties

Whiteite-(MnMnMn) forms sugary aggregates of blade-like crystals (Fig. 1) and epitaxial overgrowths on whiteite-(CaMnMn). The blades are in orthogonal orientation (Fig. 2). They have widths of up to 20 μm, and lengths of up to 100 μm. The blades are flattened on {001} and elongated along [010]. A crystal structure analysis showed the presence of twinning by 180° rotation about [100]. The crystals are colourless to very pale brown, with a white streak. The calculated density is 2.82 g·cm^{-3} for the empirical formula and single-crystal unit-cell volume.

Optically, whiteite-(MnMnMn) crystals are biaxial (–), with α = 1.599(2), β = 1.605(2) and γ = 1.609(2) (white light). The calculated 2V is 78.2°. Dispersion and pleochroism were not observed. The optical orientation is $X = \mathbf{b}$. Because of the very small size of the crystals, conoscopic observation was not possible. Nor was it possible to mount a crystal for extinction measurements. Therefore, 2V could not be measured. A Gladstone–Dale calculation gave a compatibility index of 0.056 (good) based on the empirical formula and the calculated density (Mandarino, 1981).

Chemical composition

Crystals of whiteite-(MnMnMn) in the aggregate shown in Fig. 2 were analysed using wavelength-dispersive spectrometry on a JEOL JXA 8500F Hyperprobe operated at an accelerating voltage of 15 kV and a beam current of 2.6 nA. The beam was defocused to 10 μm. Analytical results (average of analyses on 18 crystals) are given in Table 1. There was insufficient material for direct determination of H_2O, so it was based upon the crystal structure analysis. The stoichiometric amount of H_2O (2 H_2O + 0.5 OH per atom of P) was included in the matrix correction.

The empirical formula based on 26 O^{2-} anions, with Fe^{2+}/Fe^{3+} determined from the structure analysis is $(Mn^{2+}_{0.59}Ca_{0.38}Na_{0.03})_{\Sigma 1.00}Mn_{1.00}(Mn^{2+}_{1.04}Fe^{3+}_{0.58}Fe^{2+}_{0.23}Zn_{0.16}Mg_{0.08})_{\Sigma 2.09}Al_{2.04}(PO_4)_{3.89}(OH)_{3.18}(H_2O)_{7.26}$.

The simplified formula is (Mn,Ca,Na)Mn(Mn,Fe^{3+},Fe^{2+},Zn,Mg)$Al_2(PO_4)_4(OH)_2 \cdot 8H_2O$. The ideal end-member formula is $Mn^{2+}Mn^{2+}Mn^{2+}_2Al_2(PO_4)_4(OH)_2 \cdot 8H_2O$, which requires MnO 34.12, Al_2O_3 12.26, P_2O_5 34.13, H_2O 19.49, total 100 wt.%.

https://doi.org/10.1180/mgm.2021.75 Published online by Cambridge University Press

Table 2. Powder X-ray diffraction data (d in Å) for whiteite-(MnMnMn). Only calculated lines with I >1.5 are listed.

I_{obs}	d_{obs}	d_{calc}	I_{calc}	hkl	I_{obs}	d_{obs}	d_{calc}	I_{calc}	hkl
49	**9.40**	9.3529	67	001	5	2.097	2.0842	3	114
4	6.98	7.0266	2	200	3	2.056	2.0485	3	223
		6.9133	3	20$\bar{1}$	13	2.025	2.0286	3	22$\bar{4}$
3	6.21	6.2276	4	110			2.0231	2	62$\bar{1}$
15	5.62	5.6047	23	11$\bar{1}$			2.0183	2	33$\bar{2}$
66	**4.92**	4.9402	34	210			2.0149	3	62$\bar{2}$
		4.9003	26	21$\bar{1}$			2.0132	5	611
		4.8452	36	111	14	1.9995	2.0088	3	521
37	**4.70**	4.6764	35	002			2.0061	2	403
19	4.138	4.0572	13	11$\bar{2}$			1.9894	11	422
		4.0297	2	31$\bar{1}$	20	1.9767	1.9735	7	61$\bar{4}$
23	3.956	3.9788	11	211			1.9642	2	40$\bar{5}$
		3.9170	13	21$\bar{2}$			1.9625	2	331
		3.8839	12	310	**26**	**1.9500**	1.9585	10	42$\bar{4}$
9	3.791	3.7550	9	40$\bar{1}$			1.9397	22	024
42	**3.513**	3.5415	16	31$\bar{2}$			1.9355	4	214
		3.5133	26	400	10	1.9213	1.9196	2	31$\bar{5}$
		3.4864	3	112			1.9141	3	21$\bar{5}$
		3.4735	2	020			1.9104	5	232
13	3.467	3.4566	28	40$\bar{2}$			1.8989	3	23$\bar{3}$
11	3.304	3.2639	15	311	**26**	**1.8844**	1.8775	20	80$\bar{2}$
3	3.119	3.1176	7	003			1.8743	2	11$\bar{5}$
4	3.042	3.0397	9	212	3	1.8055	1.7944	2	133
13	2.980	2.9938	5	21$\bar{3}$			1.7566	2	800
		2.9621	17	401	21	1.7418	1.7368	14	040
17	2.921	2.8949	12	40$\bar{3}$			1.7283	3	80$\bar{4}$
		2.8778	8	31$\bar{3}$	7	1.7068	1.7102	3	233
		2.8247	3	221			1.7084	2	14$\bar{1}$
		2.8023	3	22$\bar{2}$			1.6986	2	23$\bar{4}$
100	**2.801**	2.7885	100	022			1.6903	2	404
		2.6801	3	51$\bar{2}$	9	1.6417	1.6467	3	630
		2.6313	2	122			1.6334	2	63$\bar{3}$
3	2.626	2.6278	2	113	3	1.6133	1.6281	3	042
		2.6055	5	510	**28**	**1.5680**	1.5676	13	820
15	2.558	2.5498	15	42$\bar{1}$	19	1.5528	1.5588	7	006
		2.5365	2	203			1.5569	5	440
		2.4889	2	60$\bar{1}$			1.5519	4	44$\bar{2}$
8	2.474	2.4736	2	60$\bar{2}$			1.5474	9	82$\bar{4}$
		2.4701	4	420			1.5384	2	63$\bar{4}$
		2.4502	3	42$\bar{2}$	12	1.5225	1.5199	10	424
10	2.417	2.4268	5	402	14	1.5023	1.4982	2	441
		2.4226	2	222			1.4969	9	42$\bar{6}$
		2.3991	2	22$\bar{3}$			1.4893	2	44$\bar{3}$
		2.3926	3	12$\bar{3}$			1.4811	2	802
8	2.364	2.3714	7	40$\bar{4}$	6	1.4036	1.4123	2	442
24	2.338	2.3431	12	61$\bar{1}$			1.4012	2	44$\bar{4}$
		2.3302	11	61$\bar{2}$			1.3942	2	044
		2.3115	3	11$\bar{4}$	10	1.3677	1.3624	5	822
		2.3044	2	60$\bar{3}$	11	1.3430	1.3395	2	425
5	2.216	2.1981	2	123			1.3361	4	82$\bar{6}$

The strongest lines are given in bold.

Table 3. Crystal data and structure refinement for whiteite-(MnMnMn).

Crystal data	
Formula (simplified)	$Mn^{2+}Mn^{2+}Mn^{2+}_2Al_2(PO_4)_4(OH)_2{\cdot}8H_2O$
Formula weight	825.9
Temperature (K)	100
Wavelength (Å)	0.7109
Space group	*P2/a*
a (Å)	15.024(3)
b (Å)	6.9470(14)
c (Å)	9.999(2)
β (°)	110.71(3)
Volume (Å^3)	976.2(4)
Z	2
Absorption correction	Multiscan, μ = 3.06 mm^{-1}
Data collection	
Crystal size (mm)	0.100 × 0.020 × 0.020
Theta range for data collection (°)	2.18 to 32.01
Index ranges	$-21 \le h \le 21$, $-9 \le k \le 9$, $-14 \le l \le 14$
Reflections collected	12,205
Independent reflections	2626
Reflections with $I_o > 3\sigma(I)$	2014
Refinement	
Refinement method	Full-matrix least-squares on F
Data / restraints / parameters	2626 / 0 / 170
Final R indices [$I > 3\sigma(I)$]	R_{obs} = 0.052, wR_{obs} = 0.057
R indices (all data)	R_{obs} = 0.064, wR_{obs} = 0.059
$\Delta\rho_{min}$, $\Delta\rho_{max}$ e^- Å^{-3}	0.78 and −0.66

Table 4. Atom coordinates, equivalent isotropic displacement parameters (Å^2) and bond-valence sums (BVS) for whiteite-(MnMnMn).

	Occupancy	x	y	z	U_{eq}	BVS
X	0.4Ca+0.6Mn	¼	0.96968(12)	0	0.0394(3)	1.98
*M*1	Mn	¼	0.47065(10)	0	0.0330(2)	1.96
*M*2A	Mn	½	0	½	0.0352(3)	2.45
*M*2B	Mn	¼	0.50296(9)	½	0.0331(3)	2.24
*M*3A	Al	0	0	0	0.0269(4)	2.99
*M*3B	Al	0	½	0	0.0268(4)	2.98
P1	P	0.17732(6)	0.25595(11)	0.18623(8)	0.0308(3)	5.03
P2	P	0.08098(7)	0.75109(11)	0.80545(8)	0.0311(3)	5.04
O1	O	0.26715(20)	0.2140(4)	0.1480(3)	0.0459(10)	1.86
O2	O	0.20362(19)	0.2917(3)	0.3442(2)	0.0398(9)	1.79
O3	O	0.1114(2)	0.0836(3)	0.1459(3)	0.0515(10)	1.90
O4	O	0.13335(16)	0.4340(3)	0.0917(2)	0.0331(8)	1.93
O5	O	0.18813(18)	0.7016(3)	0.8571(2)	0.0399(9)	1.90
O6	O	0.04640(18)	0.7824(3)	0.6442(2)	0.0382(9)	1.78
O7	O	0.07743(19)	0.9348(3)	0.8888(3)	0.0450(10)	1.94
O8	O	0.02530(16)	0.5866(3)	0.8387(2)	0.0342(8)	1.85
O9	OH	0.02222(17)	0.7492(3)	0.0835(2)	0.0316(8)	1.00
O10	H_2O	0.2259(2)	0.7366(4)	0.3413(3)	0.0544(12)	0.33
O11	H_2O	0.4478(2)	0.2199(4)	0.3437(3)	0.0568(12)	0.40
O12	H_2O	0.6329(2)	0.9990(3)	0.4712(3)	0.0485(11)	0.41
O13	H_2O	0.3951(2)	0.5137(3)	0.5116(3)	0.0469(10)	0.38

Crystallography

Powder X-ray diffraction data were obtained using a Rigaku R-AXIS Rapid II curved imaging plate microdiffractometer, with monochromatised Mo$K\alpha$ radiation. Observed d values and intensities were derived by profile fitting using *JADE Pro* software (Materials Data inc.) Data (in Å for Mo$K\alpha$) are given in Table 2. Unit cell parameters refined from the powder data using *JADE 2010* with whole pattern fitting are a = 15.023(15) Å, b = 6.949(15) Å, c = 10.013(14) Å, β = 110.79(3)° and V = 977(3) Å^3, with Z = 2.

A single-crystal diffraction dataset was collected initially using a laboratory Rigaku Xtal.LAB Synergy diffractometer at the School of Chemistry, University of Melbourne. Although the structure was able to be solved with the laboratory data, the minute size of the whiteite-(MnMnMn) crystals limited the number of observable reflections that could be collected therefore a data collection was carried out subsequently at the Australian Synchrotron, where the higher beam flux resulted in a doubling of the number of observable reflections. Despite the weaker data obtained using the laboratory diffractometer, it is interesting to note that the resulting mean polyhedral bond distances agreed with those obtained using the synchrotron data to within the measured standard deviations.

https://doi.org/10.1180/mgm.2021.75 Published online by Cambridge University Press

Table 5. Polyhedral bond lengths [Å] for whiteite-(MnMnMn).

X–O1 ×2	2.207(3)	*M*1–O1 ×2	2.273(3)
X–O5 ×2	2.331(2)	*M*1–O4 ×2	2.261(3)
X–O7 ×2	2.445(3)	*M*1–O5 ×2	2.131(2)
<*X*–O>	2.328	<*M*1–O>	2.222
X–O3 ×2	3.039(3)		
*M*2A–O6 ×2	2.035(2)	*M*2B–O2 ×2	2.073(2)
*M*2A–O11 ×2	2.127(3)	*M*2B–O10 ×2	2.208(3)
*M*2A–O12 ×2	2.116(4)	*M*2B–O13 ×2	2.144(3)
<*M*2A–O>	2.093	<*M*2B–O>	2.142
*M*3A–O3 ×2	1.881(3)	*M*3B–O4 ×2	1.940(2)
*M*3A–O7 ×2	1.926(3)	*M*3B–O8 ×2	1.882(3)
*M*3A–O9 ×2	1.909(2)	*M*3B–O9 ×2	1.900(2)
<*M*3A–O>	1.905	<*M*3B–O>	1.907
P1–O1	1.555(3)	P2–O5	1.546(3)
P1–O2	1.507(2)	P2–O6	1.524(2)
P1–O3	1.515(3)	P2–O7	1.535(3)
P1–O4	1.555(2)	P2–O8	1.521(3)
<P1–O>	1.532	<P2–O>	1.532

A blade measuring 0.10 mm × 0.02 mm × 0.02 mm was used for the single-crystal data collection made at the macromolecular beam line MX2 of the Australian Synchrotron (Aragao *et al.*, 2018). Data were collected using a Dectris Eiger 16M detector and monochromatic radiation with a wavelength of 0.7109 Å. The crystal was maintained at 100 K in an open-flow nitrogen cryostream. Refined unit cell parameters are given in Table 3.

The refinement of the crystal structure using *JANA2006* (Petříček *et al.*, 2014) was initiated using the published coordinates for whiteite-(CaMnMn) (Grey *et al.*, 2010). The amount of Ca from the electron microprobe (EMP) analyses was located with Mn in the *X* site and the Mn scattering curve was used for sites *M*1, *M*2A and *M*2B. Twinning by 180° rotation about **a** was implemented. Refinement with anisotropic displacement parameters for all atoms converged at $wR_{obs} = 0.057$ for 2014 reflections with $I > 3\sigma(I)$. Details of the data collection and refinement are given in Table 3. The refined coordinates, equivalent isotropic displacement parameters and bond valence sum (BVS) values (Gagné and Hawthorne, 2015) from the single crystal refinement are reported in Table 4. Selected interatomic distances are reported in Table 5. The crystallographic information file has been deposited with the Principal Editor of *Mineralogical Magazine* and is available as Supplementary material (see below).

Although the H atoms were not located during the structure refinement, the BVS in Table 4 show clearly the presence of one hydroxyl, O9, and four independent H_2O, O10 to O13.

Discussion

A projection of the structure along [010] is shown in Fig. 3. The interatomic distances in Table 5, and the calculated BVS values in Table 4 are consistent with full occupancy of *M*1 by Mn^{2+} and of *M*3A and *M*3B by Al, with a mix of 0.4Ca + 0.6 Mn^{2+} for the *X* site. Combining these occupancies with the EMP analyses gives a composition for the *M*2A + *M*2B sites of $(Mn_{0.99}Fe_{0.78}Zn_{0.15}Mg_{0.08})$. The BVS values for the *M*2 sites were used to calculate the oxidation state of the iron, giving the overall composition for *M*2 as $(Mn^{2+}_{0.99}Fe^{3+}_{0.58}Fe^{2+}_{0.23}Zn_{0.15}Mg_{0.08})$. With Mn dominant in the *X*, *M*1 and *M*2 sites the ideal end-member formula is $Mn^{2+}Mn^{2+}Mn^{2+}_2Al_2(PO_4)_4(OH)_2{\cdot}8H_2O$.

For jahnsite-subgroup minerals, we have reported previously an unusual negative correlation between the mean ionic radius (r) of the $X + M1$ cations and the unit-cell parameter a (Grey *et al.*, 2020). That is, with increasing size of the cations substituting at the *X* and *M*1 sites, the unit cell contracts along [100]. We have applied the same procedure to whiteite-subgroup minerals using the data reported in Table 6. The results are plotted in Fig. 4, where they are compared with the previously published results for jahnsite-subgroup minerals. The linear trendlines ($R^2 \approx 0.90$) have similar negative slopes for both subgroups, with the line for whiteite-subgroup minerals being displaced to lower a values, reflecting the smaller cations occupying the *M*3 sites (Al^{3+} versus Fe^{3+}) that separate the *X* and *M*1 cations along [100].

The negative correlation between a and $\langle r_X + r_{M1} \rangle$ was explained in terms of rotations of the *M*3 centred octahedra

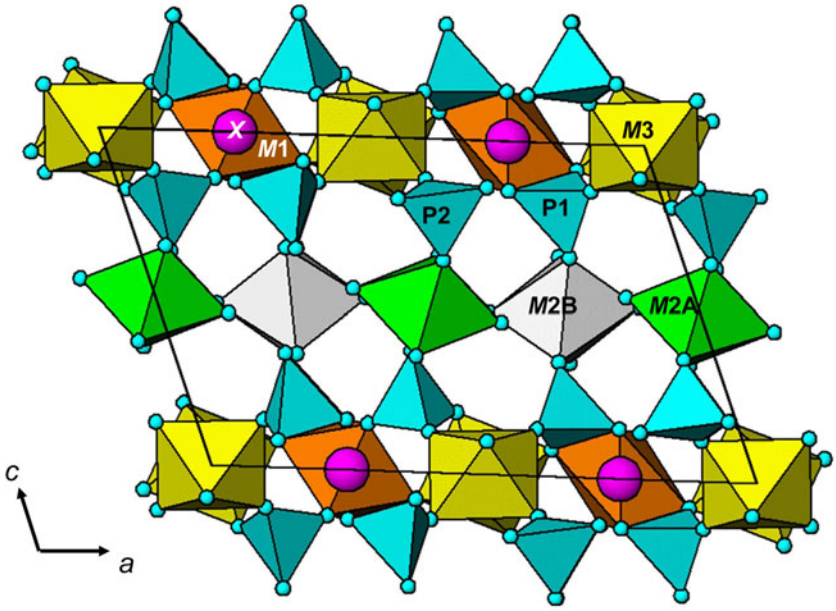

Fig. 3. [010] projection of the structure of whiteite-(MnMnMn) using *ATOMS* (Dowty, 2006).

https://doi.org/10.1180/mgm.2021.75 Published online by Cambridge University Press

Table 6. Crystallochemical data for whiteite-subgroup minerals.

	CaMgMg	CaMnMg	CaFeMg	CaMnMn	MnMnFe	MnMnMn	MnMnMg
a (Å)	14.824	14.842	14.870	14.941	15.01	15.024	15.036
b (Å)	7.030	6.976	6.978	6.949	6.89	6.947	6.941
c (Å)	9.946	10.109	9.927	10.054	10.16	9.999	9.943
β (°)	110.11	112.59	110.11	111.00	112.8	110.71	110.83
V (Å^3)	973.3	966.3	967.3	974.5	968	976.2	969.9
X	Ca	$Ca_{0.76}Mn_{0.24}$	$Ca_{0.86}Na_{0.05}$	$Ca_{0.65}Zn_{0.25}Na_{0.10}$	$Mn_{0.54}Ca_{0.46}$	$Mn_{0.59}Ca_{0.38}Na_{0.03}$	$Mn_{0.60}Ca_{0.40}$
*M*1	$Mg_{0.69}Ca_{0.31}$	Mn	$Fe_{0.81}Mg_{0.17}$	Mn	Mn	Mn	$Mn_{0.92}Mg_{0.08}$
$<r_X>$ (Å)	1.12	1.05	1.125	1.025	0.965	0.95	0.945
$<r_{M1}>$ (Å)	0.84	0.83	0.77	0.83	0.83	0.83	0.82
$<r_X + r_{M1}>$	0.98	0.94	0.945	0.928	0.897	0.89	0.882
Ref*	[1]	[2]	[3]	[4]	[5]	[6]	[7]

*[1] Kampf *et al.* (2016); [2] Grice *et al.* (1989); [3] Capitelli *et al.* (2011); [4] Grey *et al.* (2010); [5] Marzoni *et al.* (1989); [6] this study; [7] Elliott and Willis (2019).

about [010] to change the coordination number of the *X* and *M*1 cations from 6 for small cations towards 8 for large cations (Grey *et al.*, 2020). This is illustrated in Fig. 5, which shows the *X* and *M* site cations and associated coordinating polyhedra. For a large cation occupying the *X* (or *M*1) site, the *M*3A-centred octahedra are aligned with their basal edges almost parallel with **a**, and the *X* cation is 8-coordinated to 4 octahedral-edge anions ($2 \times O3 + 2 \times O7$) and 4 phosphate anions. When a small cation occupies the *M*1 (or *X*) site, the *M*3B-centred octahedra rotate about [010] to shorten bonds to two of the octahedral-edge anions (O4 in Fig. 5b) and lengthen the other pair (O8 in Fig. 5b), resulting in octahedral coordination. The octahedral rotation results in the projected width of the *M*3 octahedra onto [100] increasing from an octahedral edge distance ($=\sqrt{2}$ *M*3–O) for no rotation towards an octahedral body diagonal distance (= 2 *M*3–O) for 45° rotation. This lengthening of the projected width of the rotated *M*3 octahedra with decreasing size of *M*1 (or *X*) results in the observed increase in *a*, giving the negative correlation shown in Fig. 4.

It is important to note that the octahedra centred at sites *M*3A and *M*3B are linked by corner-connection along [010] and can rotate independently. This underpins a wide compositional diversity in jahnsite-group minerals, with cations of disparate sizes occupying the *X* and *M*1 sites, and with appropriate rotations of the *M*3A- and *M*3B-centred octahedra to meet the coordination requirements of the *X* and *M*1 site atoms. The rotations of the two independent *M*3 octahedra are of opposite sense, and they vary between 0° and 22°. The latter large rotation occurs for *M*3B in jahnsite-(NaFeMg) to give octahedral coordination about the small cation Fe^{3+} at the *M*1 site, while the *M*3A octahedron rotates only 3° to give square antiprismatic coordination about Na^+ at the *X* site (Kampf *et al.*, 2008).

Of the whiteite-subgroup minerals for which single-crystal site refinements have been published, whiteite-(CaMgMg) has the largest mean ionic radius for the *X* + *M*1 sites (Kampf *et al.*, 2016). For this mineral, the *M*3A octahedron is rotated about [010] by ~2°, giving eight Ca–O distances in the range 2.35 to 2.71 Å, whereas the *M*3B octahedron is rotated by 18°, giving six Mg–O distances in the range 2.09 to 2.22 Å. Whiteite-(MnMnMn) has the *M*3A octahedron rotated by 8° giving six Mn–O distances for the *X* site in the range 2.21 to 2.44 Å with two further Mn–O distances much longer at 3.04 Å. The *M*3B octahedron is rotated by 18°, giving six Mn–O at the *M*1 site in the range 2.12 to 2.27 Å. The overall greater rotation of *M*3 octahedra in whiteite-(MnMnMn) compared with whiteite-(CaMgMg) due to smaller mean *X* plus *M*1 cations is manifested in an increase in *a* from 14.824(2) to 15.024(3) Å.

The tendency in jahnsite-group minerals for the coordination number of the *X*-site cation to increase from six to eight as the size of the *X*-site cation increases, with a concomitant decrease

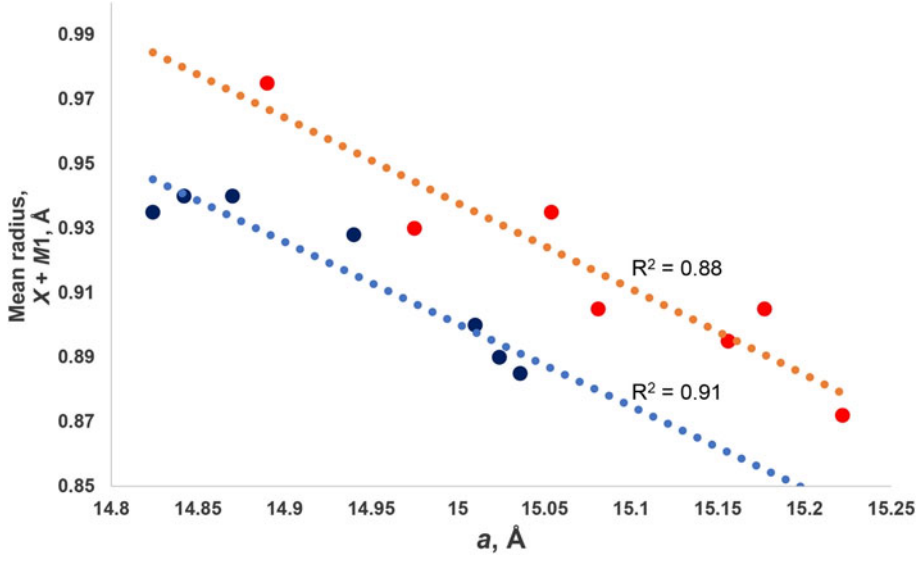

Fig. 4. Plots of mean ionic radius for *X* + *M*1 site cations *vs*. *a*. The upper plot is for jahnsite-subgroup species (from Grey *et al.*, 2020) and lower plot is for whiteite-subgroup species (data in Table 6).

https://doi.org/10.1180/mgm.2021.75 Published online by Cambridge University Press

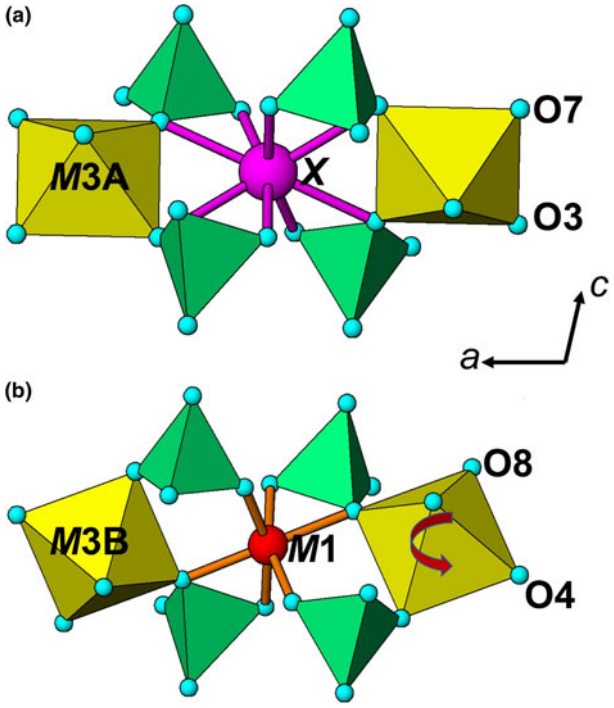

Fig. 5. Coordination environment for (a) the *X*-site cation, at $y = 0$ and (b) for the *M*1-site cation, at $y = 0.5$.

in the unit-cell size along **a** is analogous to the effect of applying external pressure. It can be described as a chemical pressure effect. This effect in jahnsite-group minerals is controlled indirectly by the substituting cation size, via the intermediary of *M*3-centred octahedral rotations, and has an analogue in negative thermal expansion (Grima *et al.*, 2006). In the jahnsite-group minerals, it is increasing cation size, rather than heating, that induces octahedral rotations and brings about anisotropic contraction of the unit cell parameters.

Supplementary material. To view supplementary material for this article, please visit https://doi.org/10.1180/mgm.2021.75

Acknowledgements. This research was undertaken in part using the MX2 beamline at the Australian Synchrotron, part of ANSTO, and made use of the Australian Cancer Research Foundation (ACRF) detector. We thank Cameron Davidson for the preparation of samples for EMP analyses.

References

Aragao D., Aishima J., Cherukuvada H., Clarken R., Clift M., Cowieson N.P., Ericsson D.J., Gee C.L., Macedo S., Mudie N., Panjikar S., Price J.R., Riboldi-Tunnicliffe A., Rostan R., Williamson R. and Caradoc-Davies T.T. (2018) MX2: a high-flux undulator microfocus beamline serving both the chemical and macromolecular crystallography communities at the Australian Synchrotron. *Journal of Synchrotron Radiation*, **25**, 885–891.

Capitelli F., Chita G., Cavallo A., Bellatreccia F. and Della Ventura G. (2011) Crystal structure of whiteite-(CaFeMg) from Crosscut Creek, Canada. *Zeitschrift fur Kristallographie*, **226**, 731–738.

Dowty E. (2006) *ATOMS*. Shape Software, Kingsport, Tennessee, USA.

Elliott P. and Willis A.C. (2019) Whiteite-(MnMnMg), a new jahnsite-group mineral from Iron Monarch, South Australia: Description and crystal structure. *The Canadian Mineralogist*, **57**, 215–223.

Gagné O.C. and Hawthorne F.C. (2015) Comprehensive derivation of bond-valence parameters for ion pairs involving oxygen. *Acta Crystallographica*, **B71**, 562–578.

Grey I.E., Mumme W.G., Neville S.M., Wilson N.C. and Birch W.D. (2010) Jahnsite-whiteite solid solutions and associated minerals in the phosphate pegmatite at Hagendorf-Süd, Bavaria, Germany. *Mineralogical Magazine*, **74**, 969–978.

Grey I.E., Keck E., Kampf A.R., MacRae C.M., Cashion J.D. and Glenn A.M. (2020) Jahnsite-(CaMnZn) from the Hagendorf Süd pegmatite, Oberpfalz, Bavaria, and structural flexibility of jahnsite-group minerals. *Mineralogical Magazine*, **84**, 547–553.

Grey I.E., Smit, J.B., Kampf A.R., Mumme W.G., Macrae C.M., Riboldi-Tunnicliffe A., Boer S. and Glenn A.M. (2021) Whiteite-(MnMnMn), IMA 2021-049. CNMNC Newsletter 63, *Mineralogical Magazine*, **85**, https://doi.org/10.1180/mgm.2021.74

Grice J.D., Dunn P.J. and Ramik R.A. (1989) Whiteite-(CaMnMg), a new mineral species from the Tip Top pegmatite, Custer, South Dakota. *The Canadian Mineralogist*, **27**, 699–702.

Grima J.N., Zammit V. and Gatt R. (2006) Negative thermal expansion. *Xjenza – Journal of the Malta Chamber of Scientists*, **11**, 17–29.

Kampf A.R., Steele I.M. and Loomis T.A. (2008) Jahnsite-(NaFeMg), a new mineral from the Tip Top mine, Custer County, South Dakota: Description and crystal structure. *American Mineralogist*, **93**, 940–945.

Kampf A.R., Adams P.M. and Nash B.P. (2016) Whiteite-(CaMgMg), $CaMg_3Al_2(PO_4)_4(OH)_2.8H_2O$, a new jahnsite-group mineral from the Northern Belle mine, Candelaria, Nevada, U.S.A. *The Canadian Mineralogist*, **54**, 1513–1523.

Kampf A.R., Alves P., Kasatkin A. and Skoda R. (2019) Jahnsite-(MnMnZn), a new jahnsite-group mineral, and formal approval of the jahnsite group. *European Journal of Mineralogy*, **31**, 167–172.

Kampf A.R., Celestian A.J. and Nash B.P. (2021) Jasonsmithite, a new phosphate mineral with a complex microporous framework, from the Foote mine, North Carolina, U.S.A. *American Mineralogist*, **106**, 174–179.

Mandarino J.A. (1981) The Gladstone-Dale relationship: Part IV. The compatibility concept and its application. *The Canadian Mineralogist*, **19**, 441–450.

Marzoni Fecia Di Cossato Y., Orlandi P. and Vezzalini G. (1989) Rittmanite, a new mineral species of the whiteite group from the Mangualde granitic pegmatite, Portugal. *The Canadian Mineralogist*, **27**, 447–449.

Moore P.B. and Ito J. (1978) I. Whiteite, a new species, and a proposed nomenclature for the jahnsite-whiteite complex series, II. New data on xanthoxenite. III. Salmonsite discredited. *Mineralogical Magazine*, **42**, 309–323.

Petříček V., Dušek M. and Palatinus L. (2014) Crystallographic Computing System JANA2006: General features. *Zeitschrift fur Kristallographie*, **229**, 345–352.